AIP Advances

Lowering the sintering temperature of calcium manganate for thermoelectric applications

Cite as: AIP Advances **12**, 085116 (2022); https://doi.org/10.1063/5.0098015
Submitted: 24 May 2022 • Accepted: 20 July 2022 • Published Online: 19 August 2022

Sophie Bresch, Björn Mieller, Ralf Moos, et al.

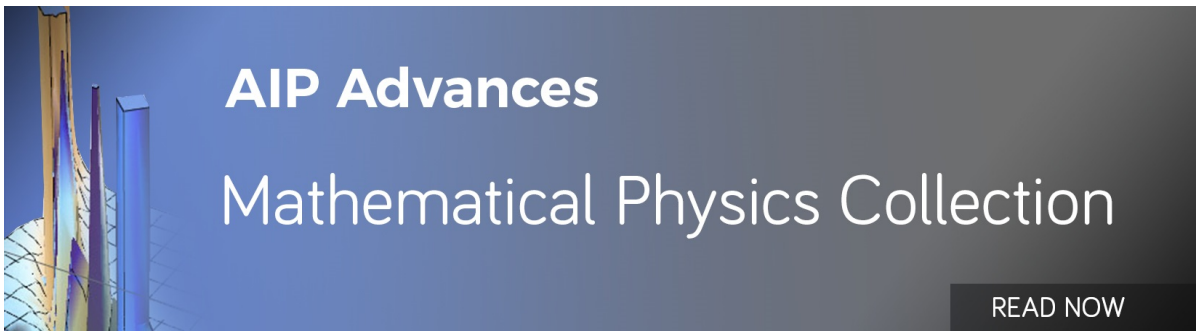

Lowering the sintering temperature of calcium manganate for thermoelectric applications

Cite as: AIP Advances 12, 085116 (2022); doi: 10.1063/5.0098015
Submitted: 24 May 2022 • Accepted: 20 July 2022 •
Published Online: 19 August 2022

Sophie Bresch,[1a)] Björn Mieller,[1] Ralf Moos,[2] and Torsten Rabe[1]

AFFILIATIONS

[1] Bundesanstalt für Materialforschung und -prüfung (BAM), Division advanced multi-materials processing, Berlin 12205, Germany
[2] Department of Functional Materials, University of Bayreuth, Bayreuth 95447, Germany

[a)] **Author to whom correspondence should be addressed:** sophie.bresch@bam.de

ABSTRACT

This study combines three different approaches to lower the sintering temperature of Sm-doped $CaMnO_3$ to save energy in production and facilitate co-firing with other low-firing oxides or metallization. The surface energy of the powder was increased by fine milling, sintering kinetics were enhanced by additives, and uniaxial pressure during sintering was applied. The shrinkage, density, microstructure, and thermoelectric properties were evaluated. Compared to micro-sized powder, the use of finely ground powder allows us to lower the sintering temperature by 150 K without reduction of the power factor. By screening the effect of various common additives on linear shrinkage of $CaMnO_3$ after sintering at 1100 °C for 2 h, CuO is identified as the most effective additive. Densification at sintering temperatures below 1000 °C can be significantly increased by pressure-assisted sintering. The power factor at room temperature of $CaMnO_3$ nano-powder sintered at 1250 °C was 445 μW/(m K^2). Sintering at 1100 °C reduced the power factor to 130 μW/(m K^2) for $CaMnO_3$ nano-powder, while addition of 4 wt. % CuO to the same powder led to ~290 μW/(m K^2). The combination of fine milling, CuO addition, and pressure-assisted sintering at 950 °C resulted in a power factor of ~130 μW/(m K^2). These results show that nano-sized powder and CuO addition are successful and recommendable strategies to produce $CaMnO_3$ with competitive properties at significantly reduced temperatures and dwell times.

INTRODUCTION

In the field of energy harvesting, thermoelectric generators are an attractive solution to transform excess heat into electrical power for low power applications, such as sensors or data transfer.[1] The physical basis for this energy conversion is the Seebeck effect. It describes the formation of a thermoelectric voltage across a temperature gradient in a material. Suitable materials are characterized by a high absolute value of the Seebeck coefficient, S, and a high electrical conductivity, σ. In the case of a quasi-unlimited heat source (energy harvesting from waste heat), the thermal conductivity, κ, plays only a minor role.[2] For highly efficient energy recovery applications, κ should be as low as possible. Thermoelectric materials can either be optimized regarding the power factor $PF = S^2 \cdot \sigma$ or regarding a dimensionless figure of merit $ZT = (PF \cdot T)/\kappa$, where T is the absolute temperature. Energy harvesting requires materials with an optimized PF and energy recovery with an optimized ZT, respectively.

For high-temperature applications above 700 °C, chalcogenides, Half-Heusler compounds, clathrates, and oxides can be considered.[3] The oxides are generally characterized by good oxidation stability but somewhat lower ZT. In comparison with other n-type oxides ($S < 0$) for high temperatures, calcium manganate ($CaMnO_3$) is seen among the most suitable materials.[4,5] Its electrical conductivity can be improved by increasing its charge carrier density by doping the Ca site[6–8] and at the Mn site.[9–11] Sintering of $CaMnO_3$ from micro-sized powder is typically performed between 1200 and 1350 °C,[6,8,12] whereas a peak temperature of 1350 °C still leads to a porosity of more than 10 %.[13]

A lower sintering temperature would save costs and energy in production. Furthermore, it will open up possibilities for co-firing with Ag-based metallization and high-performance p-type oxides, such as calcium cobaltite with a sintering temperature limited to 920 °C.[14] To decrease the sintering temperature, the driving force for sintering or the sintering kinetics must be increased. The driving force for sintering can be enhanced by increasing the chemical

potential of the powder, by increasing the surface energy of the powder, or by applying a pressure during sintering. Reaction-sintering increases the chemical potential and, thus, minimizes the porosity from 28 % to 18 % at a sintering temperature of 1250 °C.[15] Sanmathi *et al.*[13] decreased the sintering temperature of $CaMnO_3$ to 1100 °C by using nano-sized powder instead of micro-sized powder (higher surface energy). Hot-pressing of $CaMnO_3$ was performed by Kohri *et al.*,[16] though the influence on the microstructure or sintering temperature was not described.

A very efficient way to lower the sintering temperature of a ceramic material is to introduce a liquid phase that accelerates the sintering kinetics. The liquid phase should be of low viscosity. The base material should be well wetted by the liquid phase, dissolved in it, and then precipitate. Two types of additives can be distinguished: low-melting additives and additives that form a eutectic with the base material. The latter is also referred to as reactive liquid phase sintering.[17] Multiphase systems (ternary or higher) typically have lower melting temperatures than binary systems. Typical low-melting additives for functional ceramics are Li_2O,[17] LiF,[18] B_2O_3,[19] Bi_2O_3,[20] and BBSZ. The latter is a specifically developed glass for liquid phase sintering that is characterized by a low-viscosity melt and high solubility for many different ions. It has been successfully applied to various base materials.[21–23] Typical reactive additives are CuO,[17] NiO,[24] and ZnO.[25] There are only few studies on sintering additives for $CaMnO_3$ with no general overview provided by any of the studies. Hence, the present research elaborates on a general overview of sintering additives for $CaMnO_3$.

Reimann *et al.* used 2 wt. % CuO to lower the sintering temperature of $CaMnO_3$ from 1300 °C to 1050 °C.[26] At similar relative densities, S and κ remained stable, but σ decreased by about 1000 S/m in the low-firing sample. Other amounts of CuO were not considered in this study. Ferreira *et al.*[27] reported the use of K_2CO_3 but observed only a minor decrease in porosity at 1300 °C. Park *et al.*[28] investigated the addition of 0.2–2.0 mol. % Bi_2O_3. The reported microstructures showed a decrease in porosity in combination with grain growth at 1300 °C. However, the study did not provide details about porosity or shrinkage curves.

The present study aims to reduce the sintering temperature of $Ca_{0.98}Sm_{0.02}MnO_3$ (CMO) from 1250 °C to 920 °C by combining nano-sized powder, pressure-assisted sintering, and CuO as the sintering additive. The experiments include an experimental screening of various common sintering additives by evaluating their influence on the shrinkage behavior of CMO. For CuO, amounts and sintering temperatures are varied. Samples are prepared from micro-sized and nano-sized powder. Microstructure and thermoelectric properties are evaluated.

EXPERIMENTAL

For the screening of different sintering additives, $Ca_{0.98}Sm_{0.02}MnO_3$ (CMO) was used as a base material. Based on the work of Reimann *et al.*,[26] 2 wt. % of sintering additives were added to the CMO powders. Stochiometric amounts of $MnCO_3$ (≥99.9 %, Aldrich Chemistry), $CaCO_3$ (99 %, low-alkali, Riedel-de Haën), and $Sm(OH)_3$ (99.9 %, Alfa-Vernon) were attrition milled (moliNEx, Netzsch) and then calcined for 2 h at 1250 °C in air. The calcined powder was crushed by dry milling in a planetary ball mill (Pulverisette 5, Fritsch) and subsequent attrition milling for additional 15 min to obtain micro-sized powder (d_{50} = 2 μm by the laser diffraction method) and for 4 h to obtain nano-sized powder (d_{VSSA} = 100 nm calculation by the specific surface and skeletal density). As sintering additives, 0.1 g (2 wt. %) of Li_2O, LiF, B_2O_3, Bi_2O_3, BBSZ, CuO, NiO, ZnO, or binary/ternary mixtures with CuO (see Table S1 of the supplementary material for suppliers) were mixed with 5 g of CMO for 15 min in a 3D shaker mixer (Turbula, Willy A. Bachofen AG). For further investigations, 4 wt. % CuO was added directly during attrition milling of the calcined powder.

Rods with 18 mm length and 5 × 5 mm^2 cross section were uniaxially dry pressed with 60 MPa. The rods were sintered in a box furnace (FHT 1750, Ceram AIX) at peak temperatures between 950 °C and 1300 °C for 2 h. The overall heating rate was 5 K/min, except in the temperature regime between 850 °C and 950 °C (1 K/min). The final shrinkage was measured using a caliper. Sintered density and open porosity were determined by buoyancy weighing according to Archimedes. The relative density of reference samples and samples with 4 wt. % CuO was determined using calculated true densities of 4.5 g/cm^3 and 4.55 g/cm^3, respectively.

Shrinkage curves were measured using a push-rod dilatometer (DIL402c, Netzsch) with a contact force of 0.25 N and a heating rate of 5 K/min. The wetting behavior of sintering additives on CMO substrates was analyzed with heating microscopy (EMI 301, Hesse Instruments) with a heating rate of 5 K/min and a frame rate of 120 s. The microstructure was analyzed by scanning electron microscopy (SEM, Gemini Supra 40, Zeiss) in combination with energy dispersive x-ray spectroscopy (EDX, NSS 3.1, Thermo). S and σ at room temperature were measured using a laboratory setup. The setup and measurement method are described in detail by Bresch *et al.*[15] κ was calculated as the product of heat capacity, thermal diffusivity, and density. The thermal diffusivity was measured in air three times per sample using a laser flash system (LFA 457, Netzsch). Differential scanning calorimetry (STA449F3, Netzsch) in platinum crucibles and nitrogen atmosphere was performed to determine the heat capacity. PF and ZT were calculated according to their definition given in the Introduction. S and σ at elevated temperatures were additionally measured using a laboratory setup comprehensively described by Stöcker *et al.*[29]

To support densification at low sintering temperatures, tape-cast and laminated CMO samples were pressure-assisted sintered. The CMO laminates were sandwiched between SiC setter plates, with CMO and SiC separated by a zirconia release tape. A uniaxial pressure of 7.5 MPa was applied up to maximum temperatures between 880 °C and 950 °C using a sintering press (PHP-630, ATV Technologie GmbH). For details about sample preparation and heating profiles, see the supplementary material (S2 and Table S3).

RESULTS

Shrinkage measurements

The results of the broad screening of sintering additives with respect to final linear shrinkage are shown in Fig. 1. After firing at 1100 °C, the linear shrinkage of a CMO reference prepared from micro-sized powder without additives amounts to 4 %. A reference prepared from nano-sized powder exhibits 15 % final shrinkage. The sintering additives were therefore added to the nano-sized powder.

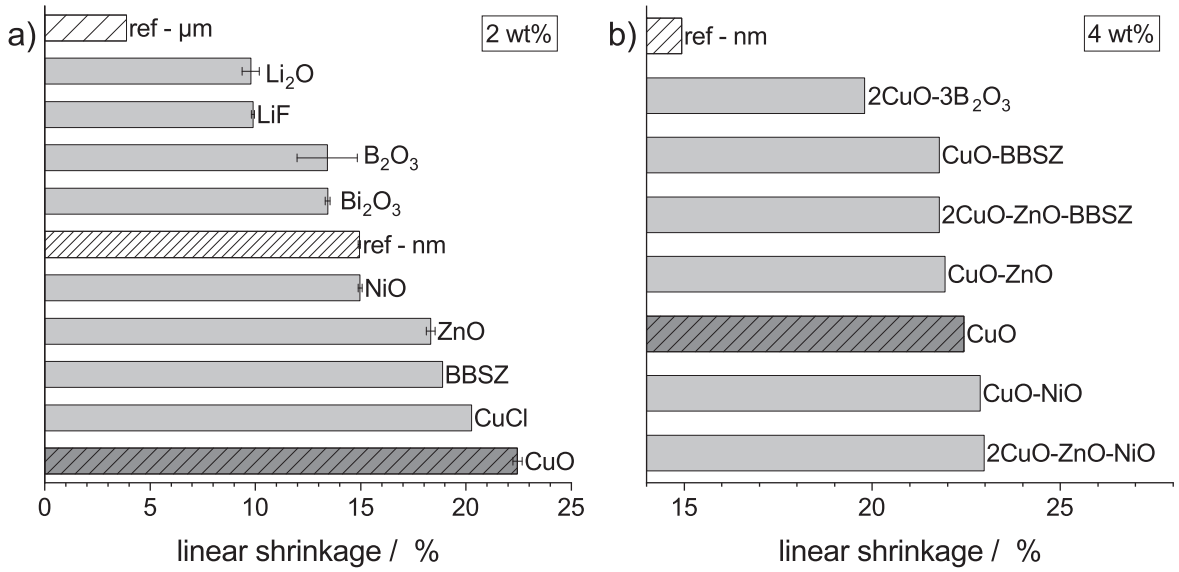

FIG. 1. Final linear shrinkage of CMO bars from nano-sized powder with different sintering additives after firing at 1100 °C: (a) 2 wt. % and (b) 4 wt. %. References from pure micro- and nano-sized powder in white with black stripes.

In comparison to the reference, only the addition of 2 wt. % ZnO, BBSZ glass, CuCl, or CuO resulted in a significant increase of shrinkage [Fig. 1(a)]. CuCl led to undesired formation of a crystallized surface layer and was therefore not considered for subsequent optimization. Addition of CuO resulted in the highest final shrinkage of 22.4 % with no open porosity. Binary or higher compounds are expected to have a lower melting point than single additives. Therefore, higher densification for the sintering additive mixtures with CuO compared to pure CuO was expected in Fig. 1(b). This could be only proven for mixtures containing CuO and NiO, though the gain in final shrinkage was less than 1 %.

Shrinkage curves of micro- and nano-sized powder, of CMO with BBSZ glass as an example of a low-melting additive, and of CMO with different variations of CuO as the reactive additive are shown in Fig. 2. The green density of bars from micro-sized powder (2.5 g/cm^3) is higher than that of bars from nano-sized powder (2.1 g/cm^3). Nano-sized powder shifts the shrinkage curve to lower temperatures compared to micro-sized powder. The addition of 2 wt. % BBSZ to nano-sized powder decreases the temperature of the maximum shrinkage rate from 1160 °C to 1080 °C. All variations of CuO addition have a stronger effect on the shrinkage rate and the final shrinkage than that of BBSZ glass. The temperatures of the maximum shrinkage rate are shifted in the range of 1030 °C even for micro-sized powder. With the increasing amount of CuO addition, the shrinkage curves are shifted to lower temperatures. Samples with 8 wt. % CuO show cracks after sintering, and thus, 4 wt. % CuO was chosen as the optimum sintering additive within the experimental framework.

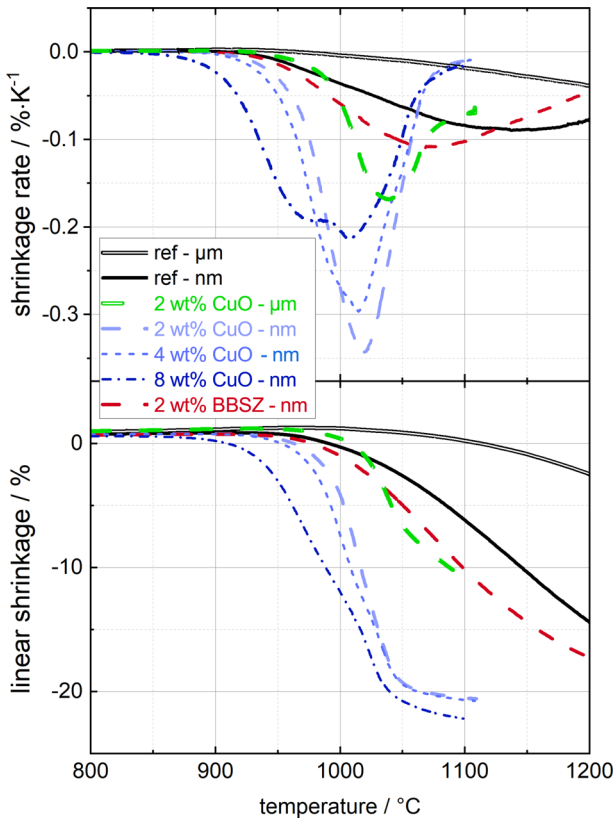

FIG. 2. Linear shrinkage and shrinkage rate over temperature for CMO from micro-sized powder (ref—μm), CMO from nano-sized powder (ref—nm), and CMO with selected additives.

Heating microscopy

As shown in Fig. 3(a), the softening point of BBSZ glass is 450 °C. BBSZ glass forms a well spreading melt on CMO at

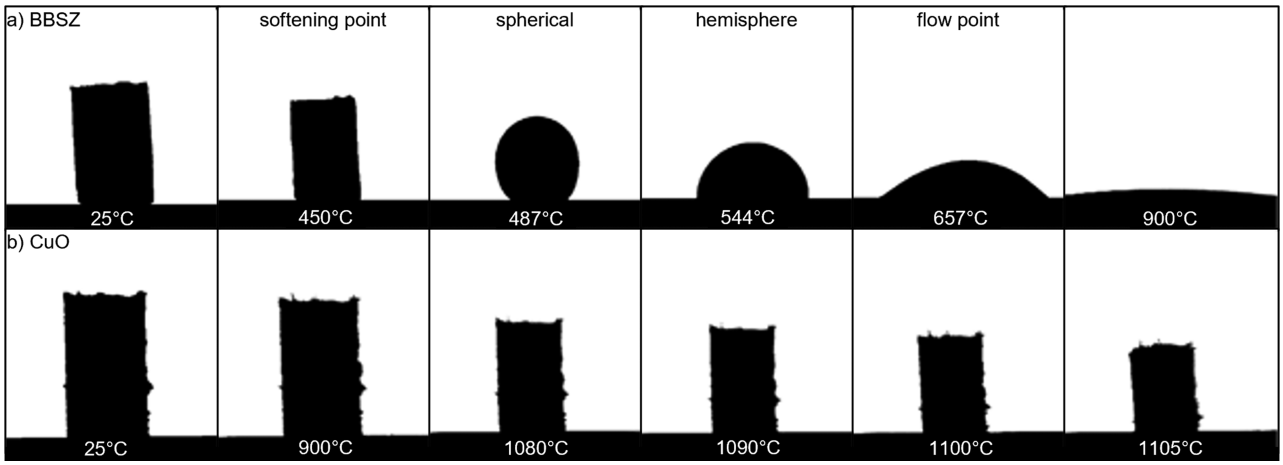

FIG. 3. Heating microscopy images of (a) BBSZ and (b) CuO on a CMO substrate.

900 °C. CuO does not melt in the analyzed temperature range [Fig. 3(b)]. Between 900 °C and 1080 °C, the CuO-block shrinks. Above 1090 °C, the CuO-block sinks into the CMO substrate.

Microstructure analysis

Microstructures of a reference sample (nano-sized powder) and a sample with 4 wt. % CuO sintered at 1100 °C are shown in Figs. 4(a) and 4(b), respectively. The reference sample shows small grains <1 μm and significant porosity. In comparison, the 4 wt. % CuO sample is dense with coarser grains (2.1 ± 0.9 μm). There are remarkable bright inclusions at the triple points at some of the grains and small pimples on the etched surfaces. EDX analysis [Fig. 4(c)] shows that the inclusions contain neither Ca nor Mn but Cu. EDX analysis shows no Sm-agglomerations. The small pimples with a mean diameter of 0.5 ± 0.2 μm are too small to be analyzed by EDX.

The microstructure resulting from sintering with 2 wt. % BBSZ glass is shown in Fig. 5. Residual porosity is distinctly observed in the specimen. Bright spots are visible on some of the grains;

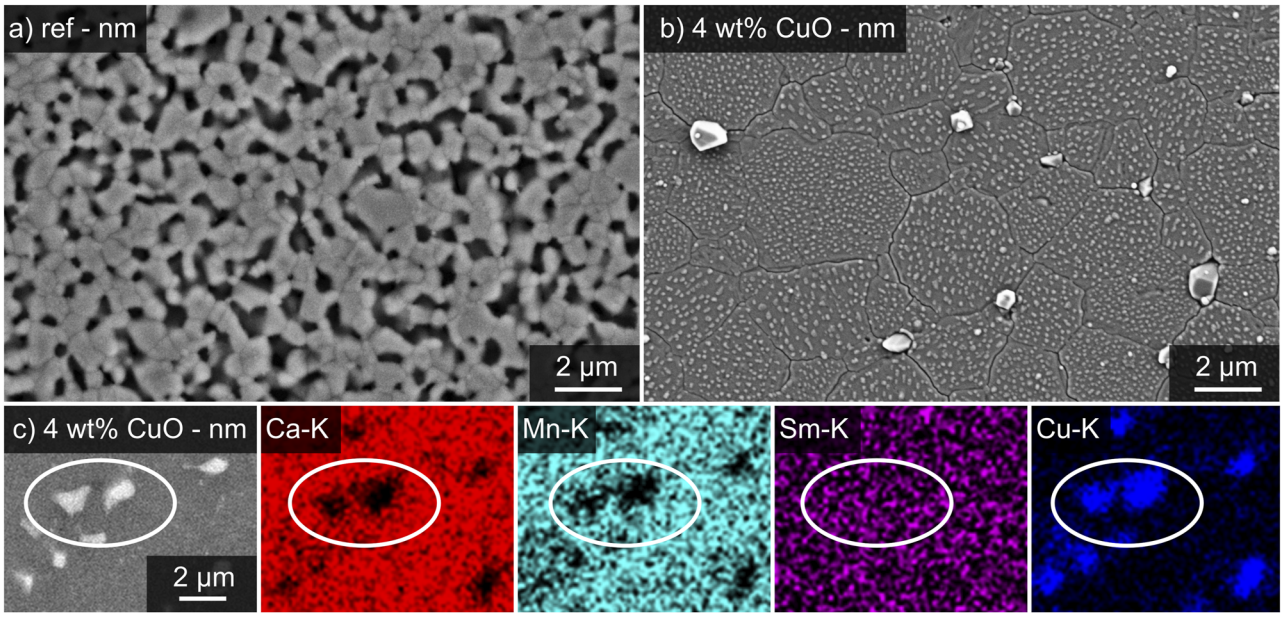

FIG. 4. SE micrograph of (a) pure CMO and (b) CMO with 4 wt. % CuO. Both specimens were thermally etched at 1000 °C for 15 min. (c) SE micrograph and elemental distribution of CMO with 4 wt. % CuO from a polished sample. All specimens sintered at 1100 °C.

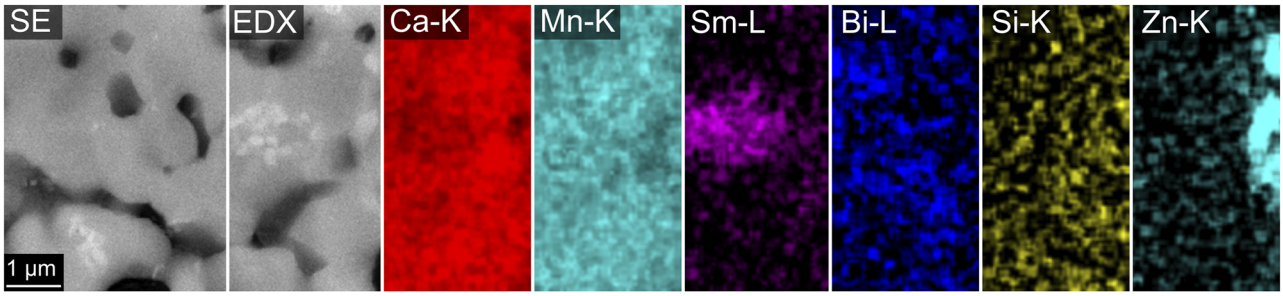

FIG. 5. SE micrograph and elemental distribution of CMO from micro-sized powder with 2 wt. % BBSZ sintered at 1100 °C.

they are either Sm-rich or Zn-rich. The main constituents of BBSZ glass, Si and Bi, appear to be homogenously distributed in the CMO microstructure.

Relative density and thermoelectric properties

Relative density and thermoelectric properties at room temperature were measured for CMO without additives (reference) and for CMO with 4 wt. % CuO after sintering at different peak temperatures (see Fig. 6). Reference samples from micro-sized powder reach only a density of 71 % after sintering at 1250 °C [Fig. 6(a)]. For nano-sized powder, the sinter density is increased to 94 %. CuO is a very effective sintering additive for CMO. After sintering at 1100 °C, samples from micro-sized powder with 4 wt. % CuO show a sinter density of 93 % even though the sintering temperature is 150 K lower than that of the micro-sized reference (71 %). Nano-sized powder with CuO reaches a relative density of 95 % at 1050 °C. A density of ~70 % is reached with a reference sample from micro-sized powder at 1250 °C, with a reference from nano-sized powder at 1100 °C, with 4 wt. % CuO at 1000 °C (nano-sized), and with additional pressure-assisted sintering already at 920 °C. σ generally decreases with the decreasing sintering temperature and decreasing sinter density [Fig. 6(b)] within the different sample groups. κ follows the trend of the relative density [Fig. 6(c)]. S remains at around −150 μV/K for samples from nano-sized powder and around −200 μV/K for samples from micro-sized powder, regardless of the sintering temperature and additive content [Fig. 6(d)]. The trend of PF vs sintering temperature follows the trend of σ [Fig. 6(e)]. The 1300 °C reference (nano-sized powder) exhibits 445 μW/(m K^2). A PF of around 130 μW/(m K^2) is reached after sintering at 1250 °C for micro-sized powder, at 1100 °C for nano-sized powder, at 1000 °C for nano-sized powder with CuO, and at 950 °C for pressure-assisted sintered nano-sized powder with CuO, respectively. The combination of pressure-assisted sintered nano-sized powder at 920 °C leads to 55 μW/(m K^2).

The high-temperature thermoelectric properties follow the same trend as the room temperature properties and are presented in the supplementary material (Fig. S4).

DISCUSSION

From the broad screening of sintering additives in Fig. 1, and with respect to the undesired surface layer resulting from CuCl addition, BBSZ and CuO were selected as the most effective additives for further investigations. The ternary additive systems show only marginal potential for better densification at 1100 °C compared to CuO and were discarded in the interest of keeping the process as simple as possible.

BBSZ glass acts as a low-melting additive and forms a well spreading melt on CMO at 900 °C [see Fig. 3(a)]. Although it is described as a particularly low-viscosity glass suitable for many functional ceramics,[22] it is not effective for CMO in lowering the onset of sintering (see Fig. 2). Thus, the BBSZ liquid phase does not support particle rearrangement of CMO in this temperature regime. Regarding the sintered microstructure, an even distribution of Si and Bi is found in the CMO (Fig. 5). This indicates that BBSZ reacts with CMO and, thus, is consumed as an additive during sintering. Si and Bi seem to be incorporated as dopants in the CMO lattice. The incorporation of Bi on Ca lattice sites has already been described for CMO.[8,30]

Based on the final linear shrinkage and the shrinkage curves, CuO is identified as the most effective sintering additive. The shrinkage curves are in good agreement with the work of Reimann *et al.*,[26] but the optimum sintering additive content is 4 wt. % in this experimental framework. Although no phase diagram of the ternary system CaO–MnO–CuO could be found in the literature, it can reasonably be assumed that CuO forms a eutectic with CMO and, thus, lowers the sintering temperature by reactive liquid phase sintering. Wetting experiments in the heating microscope showed that a CuO-block sinks into a CMO substrate, indicating a eutectic being formed at the interface [see Fig. 3(b)]. Phase diagrams for the binary systems CaO–CuO[31] and MnO–CuO[32] are available. Both show eutectics at 1012 °C for 0.8 CuO or at 1060 °C for 0.93 CuO, respectively. The eutectic in the ternary system is expected at lower temperatures.[33] Regarding the microstructure of sintered CMO with 4 wt. % CuO, the CuO was present exclusively in the triple points between the grains. This indicates that the eutectic formed during heating had separated into the components CuO and CMO during cooling.[34] The sintering additive CuO seems not to be incorporated into the CMO lattice.

S was not affected by different sintering temperatures or sintered density but by the particle size of the powder. Compared to literature values, $|S|$ reported for samples from nano-sized powder are significantly lower than that reported by Bhaskar *et al.*[6] [see Fig. 6(d)] but in good agreement with the work of Han *et al.*[35] (see Fig. S4 in the supplementary material). This may result from the use

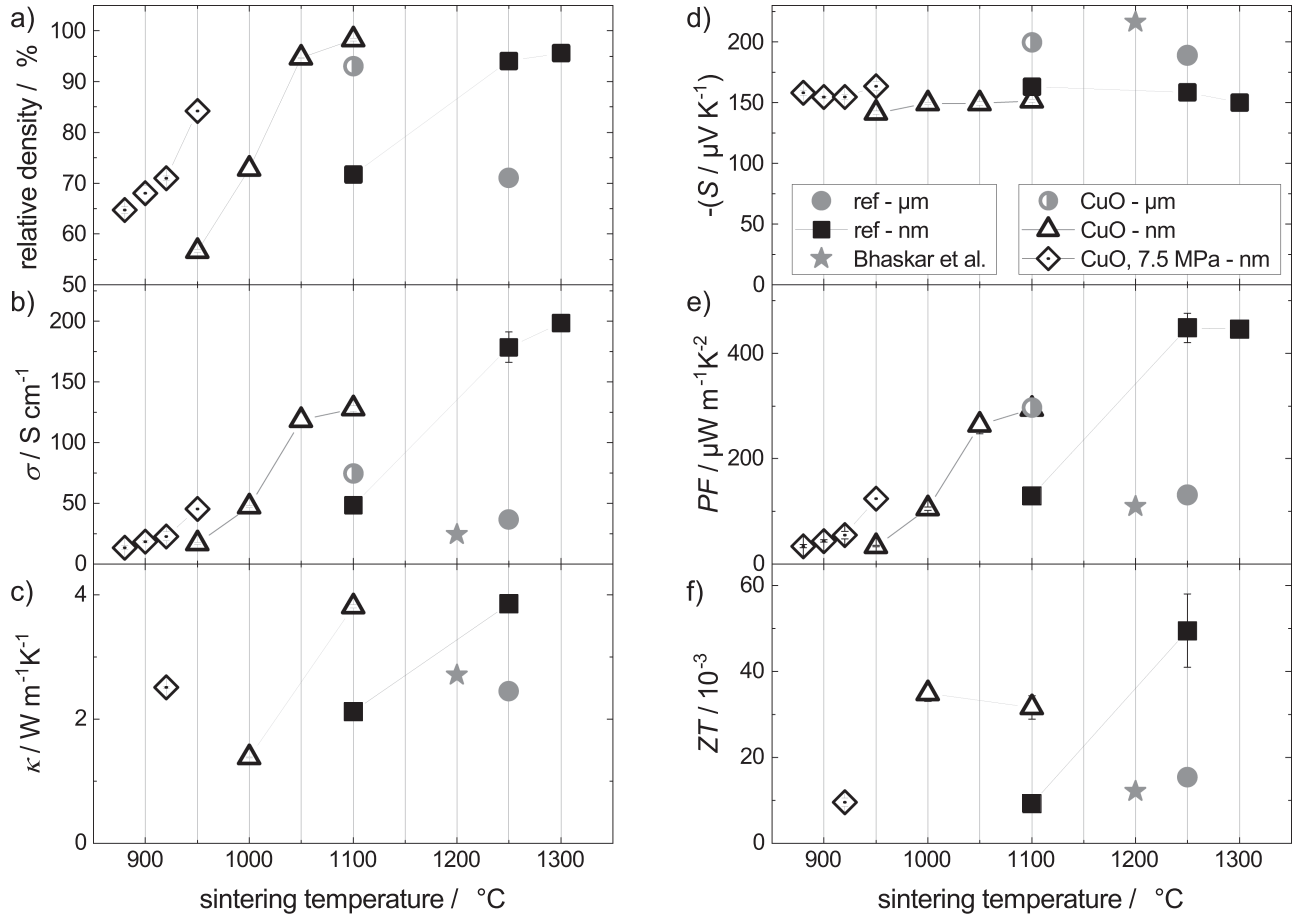

FIG. 6. (a) Relative density and (b)–(f) room temperature thermoelectric properties of CMO and CMO with 4 wt. % CuO sintered at different temperatures, (b) electrical conductivity σ, (c) thermal conductivity κ, (d) Seebeck coefficient S, (e) power factor PF, and (f) figure of merit ZT. Samples from nano-sized powder in black and from micro-sized powder in gray. Literature data taken from the work of Bhaskar *et al.*[6]

of finely ground CMO starting powder by Han and in this study. The milling process results in a better distribution of Sm in the microstructure (compare Figs. 4 and 5), lowering $|S|$.[36,37] CuO addition has no effect on S of CMO, supporting the assumption that the eutectic composition decomposes during cooling.

The sintered densities decrease with the decreasing sintering temperature as expected. CuO leads to nearly full densification of CMO down to a sintering temperature of 1050 °C. σ and κ correlate strongly with the sintered density. In samples with the same density, σ is reduced due to the addition of CuO. Reimann *et al.* reported the same behavior.[26]

Given the presence of CuO as a separate phase located at the triple junctions of the CMO grains, it appears reasonable to check the decrease of effective σ by a two-phase mixing rule.[38] Assuming σ = 0.02 S/cm for CuO[30] and a volume fraction of 2.75 %, the CMO with additive should exhibit σ = 193 S/cm at room temperature. This is much higher than the experimental values. Thus, the two-phase model does not explain the decrease in σ. Therefore, a fraction of the CuO is either assumed to form a highly resistive grain-boundary phase or to be incorporated in the CMO as a conductivity-reducing dopant (acceptor). The analysis of CuO distribution in CMO is a subject of future investigations.

Regarding the shrinkage curves, the addition of CuO (acceleration of sintering kinetics) is more effective than a finer particle size of the powder (increasing driving force for sintering) in decreasing the sintering temperature. To lower the sintering temperature below 1100 °C, both effects need to be combined. At 950 °C, the sinter density of CMO with 4 wt. % CuO can be increased from 57 % to 84 % by pressure-assisted sintering. This results in an increase of power factor by a factor of 3.6.

The thermoelectric properties as a function of the measuring temperature are shown in the supplementary material (Fig. S4). The ranking of the different material variants does not change with temperature. σ and PF achieved in this study are competitive to other published data for Sm-doped CMO. Bhaskar *et al.* reported PF ~ 100 μW/(m K^2) at 70 °C[6] after sintering at 1200 °C for 20 h. Similar values are achieved for nano-sized CMO powder with 4 wt. % CuO by pressure-assisted sintering with 7.5 MPa at 920 °C

for 2 h or by conventional sintering at 1000 °C for 2 h, respectively. This represents a reduction of 280 K or 200 K sintering temperature, respectively, and a reduction of dwell time of 18 h. Han *et al.*[35] reported a *PF* = 195 μW/(m K^2) at 300 °C for CMO nano-sized powder sintered at 1200 °C for 10 h. Similar values at 300 °C are achieved for 4 wt. % CuO after 2 h at 1100 °C in the present study. Thus, a reduction of 100 K and 8 h dwell time was achieved. The reference sample made from nano-sized powder sintered at 1250 °C exhibits 512 μW/(m K^2) at 100 °C. The *ZT*-values reported by Han *et al.*[35] are significantly higher than all samples in the current study. However, this is less decisive for an application in the field of energy harvesting.

CONCLUSION

For a high sintering temperature of 1250 °C, increasing the driving force for sintering by fine milling of the Sm-doped $CaMnO_3$ powder leads to a dense microstructure, a more homogeneous distribution of the dopant, and thus an increase in *PF* by a factor of 3.5. The achieved *PF* of 512 μW/(m K^2) at 100 °C is the highest reported for Sm-doped $CaMnO_3$ and one of the highest ever reported for doped $CaMnO_3$.[30,39]

Dense $CaMnO_3$ (relative density >95%) can be sintered in the range of 1050–1100 °C by addition of 4 wt. % CuO to the powder due to increased sinter kinetics by reactive liquid-phase sintering. At a sintering temperature of 1100 °C, micro-sized powder with CuO achieves better properties than fine milled powder without CuO.

The combination of CuO as the sintering additive, finely ground powder, and pressure assisted sintering is used to decrease the sintering temperature from 1250 °C to 950 °C by maintaining relative density and feasible thermoelectric properties in the range of literature data (sintered at 1200 °C[6]). A further decrease in the sintering temperature down to 920 °C is basically possible, whereas density and thermoelectric properties are clearly decreased. In summary, in the present study, it is shown that sintering of $CaMnO_3$ at 920 °C would provide the prerequisite to fabricate thermoelectric multilayer generators by co-sintering $CaMnO_3$ (n-type) with $Ca_3Co_4O_9$ (p-type) and Ag-based metallization.

SUPPLEMENTARY MATERIAL

See the supplementary material for supplier information of sintering additives (S1), tape casting and sample preparation for pressure-assisted sintering (S2 and S3), and temperature dependent thermoelectric properties of selected CMO samples (S3).

ACKNOWLEDGMENTS

The authors gratefully acknowledge the contribution of Fabien Giovanelli (GREMAN laboratories, Université de Tours, France), who determined the thermal conductivities.

AUTHOR DECLARATIONS

Conflict of Interest

The authors have no conflicts to disclose.

Author Contributions

Sophie Bresch: Conceptualization (lead); Data curation (lead); Formal analysis (lead); Investigation (lead); Methodology (lead); Validation (lead); Visualization (lead); Writing – original draft (equal); Writing – review & editing (lead). **Björn Mieller**: Funding acquisition (equal); Supervision (lead); Validation (supporting); Writing – original draft (lead); Writing – review & editing (supporting). **Ralf Moos**: Supervision (equal). **Torsten Rabe**: Funding acquisition (lead); Writing – original draft (supporting); Writing – review & editing (supporting).

DATA AVAILABILITY

The data that support the findings of this study are available from the corresponding author upon reasonable request.

REFERENCES

[1] N. Jaziri, A. Boughamoura, J. Müller, B. Mezghani, F. Tounsi, and M. Ismail, Energy Rep. **6**, 264–287 (2020).
[2] D. Narducci, Appl. Phys. Lett. **99**(10), 102104 (2011).
[3] M. W. Gaultois, T. D. Sparks, C. K. H. Borg, R. Seshadri, W. D. Bonificio, and D. R. Clarke, Chem. Mater. **25**(15), 2911–2920 (2013).
[4] J. W. Fergus, J. Eur. Ceram. Soc. **32**(3), 525–540 (2012).
[5] K. Koumoto, R. Funahashi, E. Guilmeau, Y. Miyazaki, A. Weidenkaff, Y. Wang, C. Wan, and X. D. Zhou, J. Am. Ceram. Soc. **96**(1), 1–23 (2013).
[6] A. Bhaskar, C.-J. Liu, and J. J. Yuan, J. Electron. Mater. **41**(9), 2338–2344 (2012).
[7] R. Kabir, D. Wang, T. Zhang, R. Tian, R. Donelson, T. Teck Tan, and S. Li, Ceram. Int. **40**(10), 16701–16706 (2014).
[8] M. Ohtaki, H. Koga, T. Tokunaga, K. Eguchi, and H. Arai, J. Solid State Chem. **120**(1), 105–111 (1995).
[9] D. Srivastava, F. Azough, R. Freer, E. Combe, R. Funahashi, D. M. Kepaptsoglou, Q. M. Ramasse, M. Molinari, S. R. Yeandel, J. D. Baran, and S. C. Parker, J. Mater. Chem. C **3**(47), 12245–12259 (2015).
[10] P. Thiel, J. Eilertsen, S. Populoh, G. Saucke, M. Döbeli, A. Shkabko, L. Sagarna, L. Karvonen, and A. Weidenkaff, J. Appl. Phys. **114**(24), 243707 (2013).
[11] S. Populoh, M. Trottmann, M. H. Aguire, and A. Weidenkaff, J. Mater. Res. **26**(15), 1947–1952 (2011).
[12] S. Lemonnier, C. Goupil, J. Noudem, and E. Guilmeau, J. Appl. Phys. **104**(1), 014505 (2008).
[13] C. S. Sanmathi, Y. Takahashi, D. Sawaki, Y. Klein, R. Retoux, I. Terasaki, and J. G. Noudem, Mater. Res. Bull. **45**(5), 558–563 (2010).
[14] S. Bresch, B. Mieller, D. Schoenauer-Kamin, R. Moos, F. Giovanelli, and T. Rabe, J. Appl. Phys. **126**(7), 075102 (2019).
[15] S. Bresch, B. Mieller, F. Delorme, C. Chen, M. Bektas, R. Moos, and T. Rabe, J. Ceram. Sci. Technol. **9**(3), 289–299 (2018).
[16] H. Kohri, M. Kato, I. J. Ohsugi, and I. Shiota, Adv. Sci. Technol. **74**, 72–76 (2010).
[17] M. Valant, D. Suvorov, R. C. Pullar, K. Sarma, and N. M. Alford, J. Eur. Ceram. Soc. **26**(13), 2777–2783 (2006).
[18] C. L. Tsai, M. Kopczyk, R. J. Smith, and V. H. Schmidt, Solid State Ionics **181**(23–24), 1083–1090 (2010).
[19] M.-H. Kim, Y.-H. Jeong, S. Nahm, H.-T. Kim, and H.-J. Lee, J. Eur. Ceram. Soc. **26**(10–11), 2139–2142 (2006).
[20] S. Wu, X. Wei, X. Wang, H. Yang, and S. Gao, J. Mater. Sci. Nanotechnol. **26**(5), 472–476 (2010).
[21] S. Bierlich, F. Gellersen, A. Jacob, and J. Töpfer, Mater. Res. Bull. **86**, 19–23 (2017).
[22] O. Dernovsek, M. Eberstein, and W. A. Schiller, J. Eur. Ceram. Soc. **21**(10–11), 1693–1697 (2001).
[23] R. Löhnert, H. Bartsch, R. Schmidt, B. Capraro, J. Töpfer, and A. Feteira, J. Am. Ceram. Soc. **98**(1), 141–147 (2015).

[24]R. Costa, N. Grünbaum, M. H. Berger, L. Dessemond, and A. Thorel, Solid State Ionics **180**(11–13), 891–895 (2009).
[25]A. Cheol-Woo, N. Sahn, R. Jungho, U. Kenji, Y. Seok-Jin, J. Soon-Jong, and S. Jae-Sung, Jpn. J. Appl. Phys. **43**(1R), 205–210 (2004).
[26]T. Reimann, A. Bochmann, A. Vogel, B. Capraro, S. Teichert, and J. Töpfer, J. Am. Ceram. Soc. **100**(12), 5700–5708 (2017).
[27]N. M. Ferreira, M. C. Ferro, A. R. Sarabando, A. Ribeiro, A. Davarpanah, V. Amaral, M. A. Madre, A. V. Kovalevsky, M. A. Torres, F. M. Costa, and A. Sotelo, J. Mater. Sci. **54**(4), 3252–3261 (2019).
[28]J. W. Park, D. H. Kwak, S. H. Yoon, and S. C. Choi, J. Alloys Compd. **487**(1–2), 550–555 (2009).
[29]T. Stöcker, J. Exner, M. Schubert, M. Streibl, and R. Moos, Materials **9**(4), 227 (2016).
[30]X. Song, S. A. Paredes Navia, L. Liang, C. Boyle, C.-O. Romo-De-La-Cruz, B. Jackson, A. Hinerman, M. Wilt, J. Prucz, and Y. Chen, ACS Appl. Mater. Interfaces **10**(45), 39018–39024 (2018).
[31]R. S. Roth, N. M. Hwang, C. J. Rawn, B. P. Burton, and J. J. Ritter, J. Am. Ceram. Soc. **74**(9), 2148–2151 (1991).
[32]F. C. M. Driessens and G. D. Rieck, Z. Anorg. Allg. Chem. **351**(1–2), 48–62 (1967).
[33]C. B. Carter and M. G. Norton, *Ceramic Materials: Science and Engineering* (Springer, New York, 2007).
[34]R. M. German, P. Suri, and S. J. Park, J. Mater. Sci. **44**(1), 1–39 (2009).
[35]L. Han, Y. Jiang, S. Li, H. Su, X. Lan, K. Qin, T. Han, H. Zhong, L. Chen, and D. Yu, J. Alloys Compd. **509**(36), 8970–8977 (2011).
[36]H. Su, Y. Jiang, X. Lan, X. Liu, H. Zhong, and D. Yu, Phys. Status Solidi A **208**(1), 147–155 (2011).
[37]Y. Wang, Y. Sui, H. Fan, X. Wang, Y. Su, W. Su, and X. Liu, Chem. Mater. **21**(19), 4653–4660 (2009).
[38]L. E. Nielsen, Ind. Eng. Chem. Fundam. **13**(1), 17–20 (1974).
[39]A. Nag and K. Sathiyamoorthy, J. Electron. Mater. **49**(12), 7036–7043 (2020).